RSC Advances

PAPER

View Article Online
View Journal | View Issue

Cite this: *RSC Adv.*, 2026, **16**, 12537

Photoelectrochemical performances of MoO_2/TiO_2 nanotube array (TNA) heterojunctions synthesized by SILAR method

Dzulhijjah Nur Meisinca and Sherly Kasuma Warda Ningsih *

Received 8th January 2026
Accepted 21st February 2026

DOI: 10.1039/d6ra00181e

rsc.li/rsc-advances

MoO_2/TiO_2 nanotube arrays (TNAs) were synthesized by the SILAR (successive ionic layer adsorption and reaction) method *via* the addition of ascorbic acid as a reductor. TNAs were synthesized using a two-step anodization method on Ti foil. Characterization was performed using UV-Vis DRS, XRD, Raman spectroscopy, and FESEM-EDX. Characterization results showed that MoO_2 modification reduced the band gap from 3.21 eV to 1.56 eV, expanding light absorption into the visible region. Photoelectrochemical tests using a potentiostat with LSV and MPA methods showed that the MoO_2/TNAs electrode had a higher current density than pure TNAs, indicating increased charge separation efficiency and photoelectrocatalytic activity.

1 Introduction

The use of photocatalysts is one effective method of treating liquid waste. Photocatalysts convert light energy into chemical energy that can produce hydroxyl radicals, which react with organic compounds (pollutants) in a redox reaction, thereby degrading the waste and restoring the water to a clear state.[1] Titanium dioxide (TiO_2) is a photocatalyst that is often used in the degradation process of organic pollutants, including dyes. TiO_2 is known as an effective photocatalyst material in the photodegradation process due to its ability to generate electron–hole pairs when exposed to UV light.[2,3]

TiO_2 can be synthesized by several methods, such as the anodization method,[4] sol–gel method, and solvothermal method.[5] However, among these methods, the anodization method has the advantage of being a simple and efficient process. The morphology of the nanotubes can be adjusted through voltage, time, and solution composition. In addition, anodization is environmentally friendly because the chemicals used can be controlled.[4] The anodization method produces TiO_2 nanotube arrays (TNAs).

TiO_2 nanotube arrays (TNAs) have superior photocatalytic advantages as photoelectrodes. These advantages are due to their large surface area and one-dimensional structure, which supports more efficient charge transport, thereby minimizing electron–hole recombination. The nanotube array structure with open tube holes at the top and perpendicular growth on the Ti metal also supports more effective electron transport, prevents electron–hole recombination, and facilitates photon energy absorption.[6]

However, the main drawback of TNAs is their relatively wide band gap, which means they can only be activated by UV light, limiting the efficiency of the photocatalytic process under sunlight.[7] To overcome this limitation, the electronic structure of the TiO_2 surface was modified with other materials that have high electrical conductivity and strong catalytic properties with other semiconductor, such as Bi_2WO_6 and Sb^{3+} doping ion,[8] construction of *Z*-scheme Bi_2O_3/CeO_2 heterojunction,[9] construction of Bi assisted CdS/TNAs,[10] heterojunction with PbS.[11] Recent studies have demonstrated that TiO_2 nanotube structures synthesized *via* anodization exhibit superior performance in gas sensing[12] and photocatalytic applications, owing to their tailored surface texture and enhanced interfacial properties using PbS/TiO_2 nanotube heterojunction synthesized by SILAR.[11]

MoO_2 is a metal oxide with good electrical conductivity and strong catalytic properties, especially in hydrogenation and oxygen reduction reactions. Synthesis of heterojunctions by adding molybdenum dioxide (MoO_2) can improve the photocatalytic performance of TiO_2. MoO_2 has a smaller band gap, ranging from 2 eV to 2.4 eV, which allows it to absorb light in a wider range, including visible light.[13] By combining MoO_2 and TiO_2 in the form of nanotubes, it is hoped that an optimal heterojunction structure will be formed. In this case, TNAs are only responsive to UV light, so they need to be modified with MoO_2 material that is responsive to visible light, thereby increasing the overall response to sunlight and optimizing performance in applications such as solar cells and pollutant processing.

In synthesizing TNAs heterojunctions with MoO_2, the SILAR (successive ionic layer adsorption and reaction) method is used.

Department of Chemistry, Faculty of Mathematics and Natural Sciences (FMIPA), Universitas Negeri Padang, Kampus Air Tawar, Padang, 25132, Indonesia. E-mail: sherly14@fmipa.unp.ac.id

The advantages of this method, apart from being simple and cost-effective, are that SILAR can control material growth well by regulating the number of process cycles, resulting in uniform and high-quality material morphology. This method is also effective in preventing electron–hole recombination, thereby optimizing performance in removing pollutants.[14]

In this research MoO_2/TNAs heterojunction was conducted using ascorbic acid as the reductor. Photoelectrochemical performances of MoO_2/TNAs have been studied.

2 Experimental section

2.1. Materials

The equipment used in this study consisted of glassware, a DC power supply, an ultrasonicator, a magnetic stirrer hot plate, a spin bar, an analytical balance, a furnace, stainless steel plates, a quartz reactor, spray bottles, Pt electrodes, Ag/AgCl reference electrodes (3 M KCl), a 19 W visible LED lamp, and a 20 W UV lamp. The materials used are titanium (Ti) plate from Shaanxi Yunzhong Metal Technology Co., Ltd, ammonium fluoride (NH_4F, Merck), ethylene glycol ($C_2H_6O_2$, Merck), NaOH, ascorbic acid ($C_6H_8O_6$), distilled water, 1000 CC and 1500 CC sandpaper, ethanol (technical grade), acetone (technical grade), sodium sulfate (Na_2SO_4, Merck), ammonium heptamolybdate tetrahydrate ($(NH_4)_6Mo_7O_{24}\cdot 4H_2O$).

2.2. Preparation of MoO_2/TNAs by the SILAR method

The synthesis process of TNAs was carried out using a two-step anodization method. The first step of anodization was done for an hour at a voltage of 40 V, and the second stage was done for 30 minutes at the same potential. After that, it was cleaned with distilled water and allowed to air dry. After that, it was heated for 2 hours at 450 °C.[15] The formation of MoO_2/TNAs was carried out using the SILAR method. TNAs were soaked in a solution of ($(NH_4)_6Mo_7O_{24}\cdot 4H_2O$) at concentrations of 10 mM, 30 mM, 50 mM, and 70 mM for 2 minutes and then washed with distilled water to remove unabsorbed ions. They were then immersed in NaOH solutions with concentrations of 10 mM, 30 mM, 50 mM, and 70 mM, rinsed with distilled water, and dried. This process was repeated 7 cycles to obtain MoO_2/TNAs catalyst samples. The samples were then immersed in ascorbic acid solutions with concentrations of 10 mM, 30 mM, 50 mM, and 70 mM at 80 °C for 60 minutes. They were then varied with calcination treatment using argon and without calcination after the SILAR process with the same cycle and concentration variations.[14]

2.3. Characterization of MoO_2/TNAs

Characterization of TNAs before and after the formation of n–p junctions with MoO_2 was analysed using XRD to determine the crystal structure. This process was carried out by comparing the XRD measurement results with the JCPDS TiO_2 and MoO_2 data. The optical properties or band gap of the photocatalyst material were analysed using UV-Vis DRS spectroscopy. The Raman shift in the sample was observed through Raman spectroscopy. Furthermore, surface analysis and heterojunction material analysis on the MoO_2/TNAs sample were carried out using FE-SEM EDX.

2.4. Photoelectrochemical performance of MoO_2/TNAs heterojunction

PEC cells are arranged in two types of configurations, namely PEC cells for testing photoelectrode activity and PEC cells for degradation production. PEC cells for testing photoelectrode activity consist of a quartz container equipped with a three-electrode system, namely the working electrode, which is TNAs and MoO_2/TNAs. The reference electrode used is Ag/AgCl, and the counter electrode is a platinum electrode. To test electrode performance, this PEC cell is equipped with a 20 W UV lamp and a 19 W visible LED lamp. The electrolyte solution used is 0.1 M Na_2SO_4. Photocurrent and photocurrent transient measurements are performed using the Linear Sweep Voltammetry (LSV) and Multi-Pulsed Amperometry (MPA) technique.

3 Results and discussion

TNAs were synthesized using a two-step anodization method by varying the anodization time in the second stage. A Ti plate was used as the anode (working electrode) and a stainless-steel plate as the cathode (counter electrode). The distance between the two electrodes was set at 1.5 cm. The anodization process in the first stage was carried out at a potential of 40 V for 60 minutes, and in the second stage, it was carried out for 30 minutes in an ethylene glycol electrolyte solution containing 0.3% wt NH_4F and 2% H_2O. This aims to study the hierarchy of the top layer and bottom tube morphology of TNAs on PEC properties. Ethylene glycol was chosen as the solvent because it has a relatively low viscosity value (1.61×10^{-2} N s m^{-1}), which facilitates ion diffusion in the solution. The TiO_2 layer will form when the Ti metal oxidizes when the electrical potential is turned on, while H_2 gas bubbles form on the stainless-steel plate. DC power supply equipment is used to provide a constant potential of 40 volts, because nanotube formation using an ethylene glycol solution is optimal at an electrical potential of 20–65 volts.

The use of a two-step anodization method in this study was based on a template-assisted approach, in which the initial structure resulting from the first stage of anodization was removed to leave a regular pattern that would serve as a template for the growth of TNAs in the second stage. This can improve the regularity of the morphology of TNAs and produce a more homogeneous and vertically oriented structure. Variations in current over time during anodization were recorded and observed using a DC power supply.

The growth process of Titanium Nanotube arrays (TNAs) through a two-stage anodization method at a constant voltage of 40 V was analyzed based on the current density curve profile over time, as shown in Fig. 1. This curve shows changes in current density in response to time during the anodization process, which is generally divided into three main parts: the initial oxide layer formation stage (barrier layer), pore formation

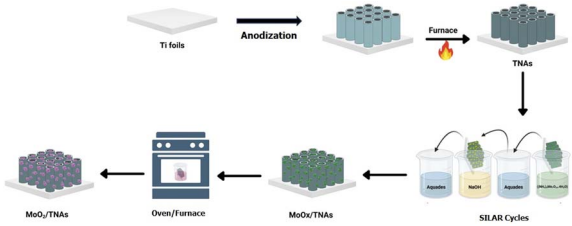

Fig. 1 Illustration of the preparation of MoO_2/TNAs.

through chemical dissolution, and the equilibrium stage or vertical pore growth.

Fig. 2 shows the anodization curve profile of TNAs prepared at 40 V for 60 minutes and 40 V for 30 minutes, indicating that the current density at an anodization potential of 40 V for 60 minutes decreased significantly from 23.33 mA cm^{-2} to 5 mA cm^{-2} in the first 30 seconds. This decrease is caused by the formation of a non-conductive TiO_2 barrier layer, which limits the flow of ions between the electrolyte and the titanium substrate, causing the anodization current to decrease. This process corresponds to the reaction:

$$Ti + 2H_2O \rightarrow TiO_2 + 4H^+ + 4e^-$$

After the initial oxide layer is formed, there is an increase in current density from 5 mA cm^{-2} to 6.67 mA cm^{-2} within 120 seconds, indicating the start of the chemical dissolution process, where fluoride ions (F^-) dissolve certain parts of the TiO_2 layer, forming small holes and pores. This process increases the conductivity of the anode because the pores formed increase the reactive surface area.[16] The reaction to form the $[TiF_6]^{2-}$ complex proceeds *via*:

$$TiO_2 + 6F^- + 4H^+ \rightarrow [TiF_6]^{2-} + 2H_2O$$

Then equilibrium occurs, characterized by a decreasing and relatively constant density current, caused by ionic current flowing through the pore site and playing a role in increasing the depth or length of the grown nanotube.

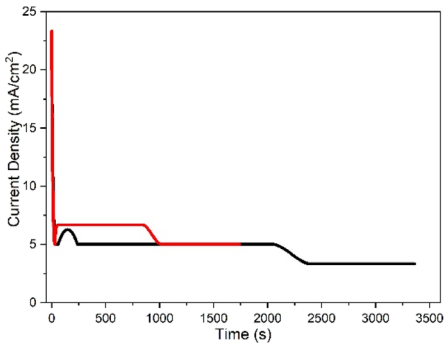

Fig. 2 Anodization curve profile TNAs ■ 40 V 60 minutes ■ 40 V 30 minutes.

Furthermore, in the second stage (40 V for 30 minutes), the current curve profile shows a pattern similar to the first stage, but there are some important differences. The current decrease in the initial part (t_1) is not as deep as in the first stage, and the current increase in the second part (t_2) occurs more quickly. This indicates that the barrier layer formation process is thinner and the electric field is more effectively distributed due to the template from the first stage of anodization. The morphology of the titanium surface, which already has a pore pattern from the previous stage, causes the electric field distribution to be more uniform, thereby accelerating the initiation of pore formation in the second stage.

The maximum current density achieved in the second stage was also slightly higher than in the first stage. This indicates that the electrochemical reaction proceeded more rapidly and intensely, potentially producing TNAs with greater length and diameter in a shorter time. Under steady-state conditions in the second stage, the current remained stable, indicating the continuous and controlled formation of pores.

Overall, these results indicate that the use of a two-step anodization method at a fixed voltage of 40 V can improve the morphological regularity of TNAs. This is demonstrated by a more stable and efficient current curve pattern in the second stage, as a result of the electric field distribution being guided by the initial structure. These observations are consistent with previous findings,[17] which state that two-stage anodization is capable of producing a more uniform and vertical nanotube structure due to the initial mold from the first anodization.

3.1. Characterization of MoO_2/TNAs heterojunction by UV-Vis DRS

Fig. 3 shows the UV-Vis DRS spectra of TNAs and MoO_2/TNAs samples prepared using the 7-cycle SILAR method at various concentrations (10 mM, 30 mM, 50 mM, and 70 mM) and thermal treatment variations (with and without argon). It can be seen that pure TNAs have high reflectance in the UV region around 380 nm, which is a characteristic feature of anatase phase TiO_2 semiconductors. Reflectance decreased significantly after modification with MoO_2 without using an argon furnace, indicating an increase in light absorption capacity, especially in the visible light range (400–700 nm).

A fairly drastic decrease in reflectance was observed in MoO_2/TNAs samples without argon furnace treatment, indicating that MoO_2 doping successfully expanded the light absorption range to the visible region and improved the photocatalytic potential of the material. The spectra of MoO_2/TNAs also show broader and more intense absorption compared to pure TNAs, indicating an increase in the interaction between visible light and the material surface.

The optical band gap value was calculated using the Tauc plot method based on the Kubelka–Munk transformation, as shown in Table 1. The optical band gap of pure TNAs was obtained to be 3.21 eV, which is consistent with the anatase TiO_2 character. After modification with MoO_2, the band gap value decreased significantly, especially at a concentration of 50 mM without argon annealing treatment, which showed a band gap

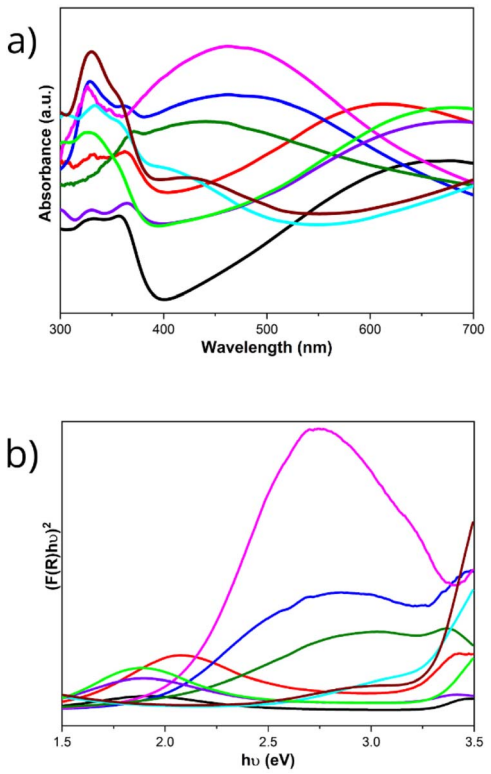

Fig. 3 (a) Spectrum UV-Vis DRS (b) Tauc plot TNAs 40 V 60 minutes 40 V 30 minutes, MoO_2/TNAs 10 mM, MoO_2/TNAs 30 mM, MoO_2/TNAs 50 mM, MoO_2/TNAs 70 mM, MoO_2/TNAs 10 mM (argon), MoO_2/TNAs 30 mM (argon), MoO_2/TNAs 50 mM (argon), MoO_2/TNAs 70 mM (argon).

of 1.56 eV, indicating that MoO_2 successfully reduced the electron excitation energy, allowing the material to absorb more light in the visible region.

Band gap reduction allows the material to absorb longer-wavelength (visible) light, not only UV light. This increases the number of absorbed photons, generating more electron–hole pairs. The reduction of the band gap contributes to photocurrent enhancement by extending light absorption into the visible region, thereby increasing the generation of photogenerated charge carriers. The higher carrier density, combined with improved interfacial charge transfer and suppressed charge recombination, leads to an overall increase in photocurrent response.[15]

Table 1 Band gap values of MoO_2/TNAs

Sample	Band gap (eV)	Sample code
TNAs 40 V 60 minutes 40 V 30 minutes	3.21	TNAs
MoO_2/TNAs 7 cycles 10 mM	3.09	Mo10
MoO_2/TNAs 7 cycles 30 mM	1.76	Mo30
MoO_2/TNAs 7 cycles 50 mM	1.56	Mo50
MoO_2/TNAs 7 cycles 70 mM	1.82	Mo70
MoO_2/TNAs 7 cycles 10 mM (argon)	3.05	Mo10A
MoO_2/TNAs 7 cycles 30 mM (argon)	2.86	Mo30A
MoO_2/TNAs 7 cycles 50 mM (argon)	3.12	Mo50A
MoO_2/TNAs 7 cycles 70 mM (argon)	3.13	Mo70A

Samples without argon furnace treatment (only ascorbic acid immersion and 80 °C oven) showed a significant narrowing of the band gap (1.56–1.82 eV at concentrations of 30–70 mM), compared to pure TNAs. Conversely, further treatment with a furnace in an argon atmosphere resulted in larger band gap values closer to those of pure TNAs, ranging from 2.86 to 3.14 eV.

This can be explained by considering the role of ascorbic acid, precursors, and thermal treatment. Ascorbic acid functions as an effective reducing agent to reduce molybdenum from a higher oxidation state (Mo^{6+} or Mo^{5+}) to Mo^{4+}, which is the form in MoO_2. After reduction, ascorbic acid also helps stabilize MoO_2 so that it does not reoxidize to the MoO_3 (Mo^{6+}) form. In addition, ascorbic acid can prevent excessive oxidation during the furnace process, resulting in a homogeneous MoO_2 layer with a sufficient level of defects. The presence of structural defects and trap states due to crystal imperfections in the MoO_2 layer without a furnace tends to reduce the band gap value due to the emergence of an intermediate energy level in the valence and conduction bands, which facilitates the excitation of electrons with lower energy.

The use of a furnace with an argon atmosphere at high temperatures aims to improve the crystallinity of the MoO_2 layer, prevent oxidation to MoO_3 with a wider band gap, and eliminate excessive defects that can cause interband energy levels. This causes the band gap value of the material to be closer to the intrinsic value of pure TNAs and reduces the intensity of mid-gap states that narrow the band gap. However, the improvement in structure actually makes the band gap less narrow than expected for photocatalytic degradation applications, as a narrow band gap allows for more effective absorption of the visible light spectrum and increases the formation of active electron–hole pairs.

Overall, treatment without an argon furnace resulted in a narrower band gap for modified MoO_2/TNAs than treatment with an argon furnace. This shows that the defect level and interband energy state (band tailing) maintained without argon annealing actually increased light absorption in the visible and near-infrared regions, thereby facilitating the photocatalytic reaction for the degradation of dyes.

The charge transfer mechanism at the MoO_2/TiO_2 interface, TiO_2 absorbs photons and produces electron–hole pairs under illumination:

$$TiO_2 + h\nu \rightarrow e_{CB}^{-}(TiO_2) + h_{VB}^{+}(TiO_2)$$

MoO_2 is metallic, while TiO_2 is an n-type semiconductor. When the two come into contact, the Fermi level equalizes, forming a Schottky barrier on the TiO_2 side. Electrons excited in the TiO_2 conduction band are spontaneously transferred to MoO_2, as MoO_2 has high conductivity and acts as an electron sink/collector. The Schottky barrier inhibits the backflow of electrons to TiO_2, significantly reducing electron–hole recombination. Electrons captured by MoO_2 are rapidly transported to

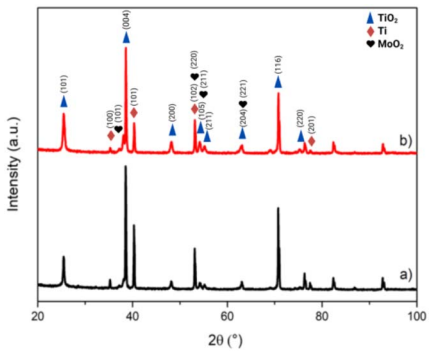

Fig. 4 Diffractogram patterns (a) TNAs 40 V 60 minutes 40 V 30 minutes (b) MoO_2/TNAs 7 cycles 50 mM.

the current collector, while holes remain in TiO_2 and participate in oxidation reactions at the electrode–electrolyte interface.[18]

3.2. Characterization of MoO_2/TNAs heterojunction by XRD

XRD characterization aims to determine the crystal structure of TNAs and MoO_2/TNAs prepared using the SILAR method. Fig. 4 shows the XRD diffractogram of pure TNAs samples with the anatase phase can be observed at 2θ: 25.5°; 38.1°; 48.1°; 54.2°; 55.2°; 63.0°; 68.9°; 70.9°; and 76.3°, which correspond to the crystal planes (101), (004), (200), (105), (211), (204), (116), and (220), as listed in the JCPDS standard no. 00-021-1272.[19] The presence of this anatase peak indicates that the TiO_2 phase formed is crystalline with a tetragonal structure. This shows that amorphous TiO_2 turns crystalline at a calcination temperature of 450 °C. The average crystallite size of TNAs was 49.15 ± 23 nm (RSD = 45.4%).

In addition to the anatase phase, titanium metal peaks were also detected at 2θ: 35.2°; 40.3°; 53.1°; and 77.3°, which are associated with crystal planes (100), (101), (102), and (201) according to JCPDS data no. 21-1294.[20] This peak originates from the Ti foil substrate used as the working electrode during the anodization process, and its presence does not interfere with the identification of the main TiO_2 phase.

For MoO_2/TNAs samples modified using the SILAR method for 7 cycles at a precursor concentration of 50 mM, in addition to the anatase and Ti peaks, several peaks characteristic of MoO_2 compounds were also identified. These peaks appeared at 2θ: 37.1°; 53.1°; 54.2°; and 63.1°, each corresponding to the crystal planes (101), (220), (211), and (221) according to JCPDS no. 86-0135.[21] The presence of these peaks confirms that MoO_2 was successfully deposited on the surface of TNAs and has a tetragonal crystalline structure. The average crystallite size of 7MoO_2/TNAs (50 mM) was 51.91 ± 10.79 nm (RSD = 20.8%).

Thus, XRD analysis shows that modification of TNAs with MoO_2 using the 7-cycle SILAR method successfully formed a heterojunction structure between anatase TiO_2 and crystalline MoO_2, without removing the anatase phase or damaging the Ti metal substrate. This structure is expected to support increased photocatalytic activity in organic compound degradation applications (Table 2).

3.3. Characterization of MoO_2/TNAs heterojunction by Raman spectroscopy

Raman spectroscopy was used to identify the crystal phase, detect active vibration modes, and evaluate structural changes in TiO_2 nanotube arrays (TNAs) before and after modification with MoO_2. The Raman spectra of TNAs and MoO_2/TNAs are shown in Fig. 5.[22]

The Raman spectrum of TNAs shows characteristic peaks of the anatase phase of TiO_2, namely the presence of a symmetric O–Ti–O stretching vibration peak appearing at 144 cm^{-1} (Eg1), Ti–O vibration peaks at 396 cm^{-1} (B1g), 513 cm^{-1} (A1g), 636 cm^{-1} (Eg) (Fig. 5a). The Raman spectrum value at 144 cm^{-1} corresponds to the Raman spectrum reference for pristine TiO_2. This indicates that the TiO_2 phase formed is the anatase phase, which is consistent with the XRD characterization results. The Eg and B1g peaks are the symmetry stretching vibration and symmetry bending vibration of the O–Ti–O bond in TiO_2, respectively. The intensity of the Eg1 peak in the two-stage anodized sample indicates a good degree of crystallinity in the

Table 2 The crystallite size of TNAs and MoO_2/TNAs

No	Photoanode	2θ (°)	FWHM (rad)	Crystal size (nm)	Average crystallite size (nm)
1	TNAs (40 V 60 minutes 40 V 30 minutes)	25.5	0.2273	35.44	49.15 ± 23 nm, (RSD = 45.4%)
		38.1	0.1299	63.98	
		48.1	0.2598	33.12	
		54.2	0.3247	27.19	
		55.2	0.2598	34.13	
		63.0	0.1299	70.97	
		68.9	0.7793	12.23	
		70.9	0.1188	81.22	
		76.3	0.1188	84.09	
2	7MoO_2/TNAs 50 mM	37.1	0.3827	37.18	51.91 ± 10.79 nm, (RSD = 20.8%)
		53.1	0.1299	53.14	
		54.2	0.3897	54.20	
		63.1	0.0974	63.11	

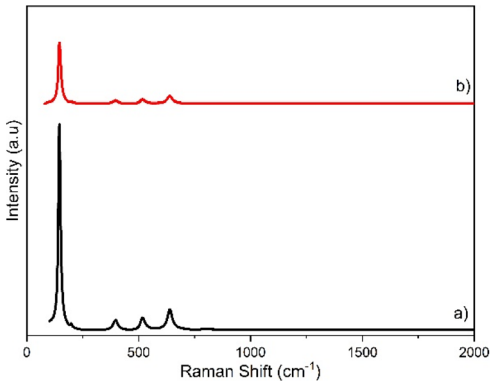

Fig. 5 Raman spectrum of (a) TNAs 40 V 60 minutes 40 V 30 minutes, (b) MoO_2/TNAs 50 mM.

TNAs structure. The higher the Eg1 intensity, the higher the crystallinity and regularity of the TiO_2 anatase structure.[23]

After the surface modification process of TNAs with MoO_2 (Fig. 5b), the six anatase peaks remained, indicating that the TiO_2 crystal structure did not change significantly due to the impregnation process. However, there was a slight shift in the Raman peak positions to 145.47 cm^{-1} (Eg1), 395.41 cm^{-1} (B1g), 517.19 cm^{-1} (A1g), and 638.75 cm^{-1} (Eg1). The shift in peak position (blueshift) to a higher wave number and peak broadening indicate an interaction between MoO_2 and the TiO_2 surface, causing a change in the local O–Ti–O bond environment but without changing the main phase of TiO_2. The increase in peak intensity in MoO_2/TNAs compared to the original TNAs reflects an increase in crystallinity or the possibility of an increase in defect sites relevant to catalytic and photoelectrochemical applications.

3.4. Characterization of MoO_2/TNAs heterojunction by FESEM-EDX

Morphological analysis of TNAs was performed using FESEM to determine the surface structure and cross-section of the formed TiO_2 tubes. Fig. 5 shows the surface morphology and cross-section of TNAs prepared by the two-step anodization method at a potential of 40 V for 60 minutes in the first step and 40 V for 30 minutes in the second step.

Fig. 6a shows uniform pore openings that are evenly distributed across the entire surface. This surface morphology indicates that the TiO_2 layer has formed consistently, with a pore size of approximately 46.39 nm. Fig. 6b shows that the TiO_2 tubes are arranged perpendicular to the substrate with a tube height of approximately 1.5 μm, indicating a highly ordered and homogeneous structure. This structure indicates that the anodization parameters used are optimal in supporting the vertical growth of TiO_2 nanotubes. The morphology of the TNAs appears to form a regular hexagonal (honeycomb) pore pattern.[15]

Fig. 6c shows the result after modification with MoO_2 using the SILAR method for 7 cycles at a concentration of 50 mM, resulting in a decrease in the average pore diameter to 38.31 nm. Fig. 5d shows that the tubes are arranged straight on

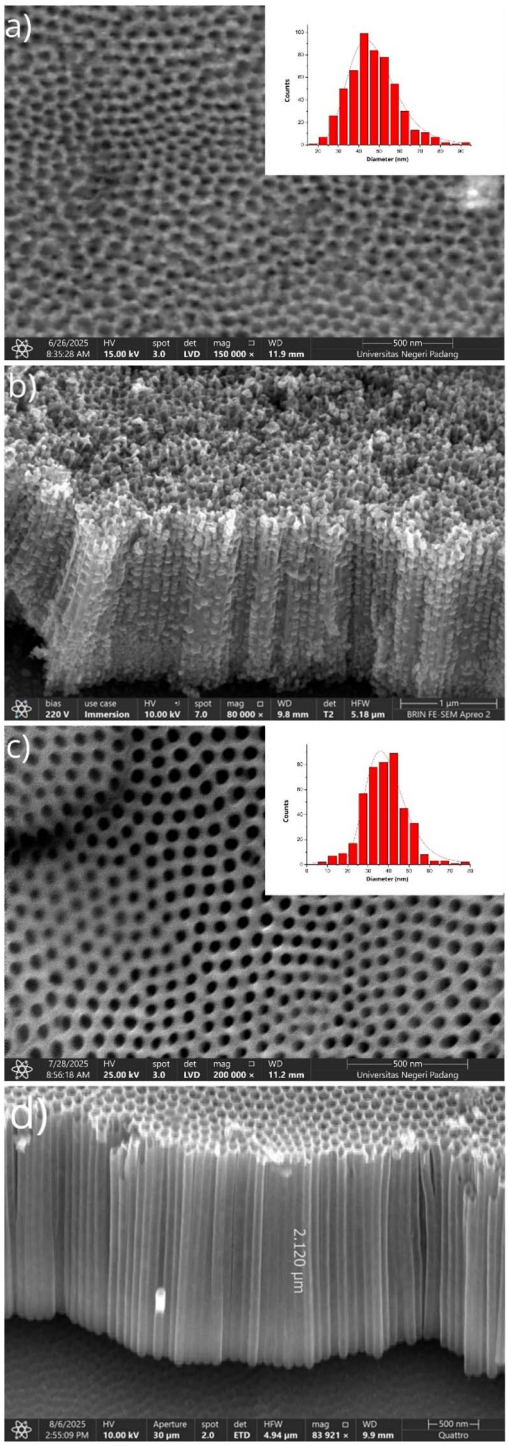

Fig. 6 FESEM images (a) surface morphology of TNAs 40 V 60 min 40 V 30 min (b) cross section of TNAs 40 V 60 min 40 V 30 min (c) surface morphology of MoO_2/TNAs 50 mM (d) cross section of MoO_2/TNAs 50 mM.

the substrate with a tube height of about 2 μm, indicating a highly ordered and homogeneous structure. This change indicates that the MoO_2 layer successfully coated the TNAs surface without damaging the formed nanotube structure. The preserved morphology with a regular pore pattern supports

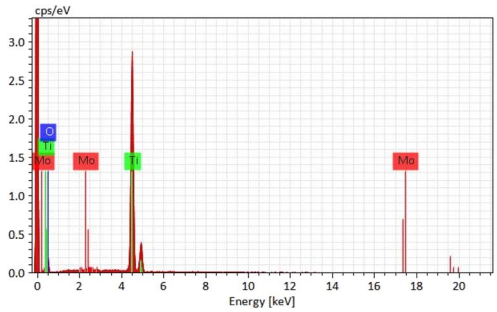

Fig. 7 EDX spectrum of 50 mM MoO_2/TNAs.

Table 3 EDX results from MoO_2/TNAs 50 mM

Element	Norm. mass concentration (%)	Norm. atomic concentration (%)
Oxygen	39.08	65.80
Titanium	60.65	34.12
Molybdenum	0.27	0.01
Sum	100.00	100.00

efficient electron transfer and optimal light absorption for photocatalyst performance.

Fig. 7 shows the EDX spectrum results of MoO_2/TNAs, which identify the presence of Ti (titanium) 34.12%, O (oxygen) 65.80%, and Mo (molybdenum) 0.01% layers, indicating the presence of TiO_2 and MoO_2 compounds in Table 3. TiO_2 nanotube arrays (TNAs) show the dominance of titanium (Ti) and oxygen (O) elements, as well as the presence of Mo (molybdenum) as a modification layer. The atomic composition of Ti and O is the dominant element with significant atomic percentages, while Mo is a thin layer covering the surface of TNAs. This indicates the success of MoO_2 coating on the surface of TiO_2 nanotube arrays, which will later act as a heterojunction in enhancing photocatalytic properties.

3.5. Characterization of MoO_2/TNAs heterojunction by LSV and MPA

The photoelectrochemical performance of TNAs does not respond well to visible light, because the photocurrent is very small compared to when illuminated by UV light. This occurs because TiO_2 has a fairly large bandgap of around 3.2 eV, so it can only absorb high-energy light such as UV. Visible light is not strong enough to activate this material, so not many electrons can be generated.[24] As shown in Fig. 8a and b, the ability of TNAs to generate electric current from light is very low. The photoelectrochemical method applied in this study is the measurement of photocurrent *versus* potential (LSV). Photocurrent is generated through the application of a potential sweep. Meanwhile, transient photocurrent is obtained from irradiation at a constant potential and specific wavelength in the form of a short light pulse (MPA), which aims to determine charge kinetics, such as the electron diffusion coefficient and the electron transport time from the photocatalyst to the substrate.

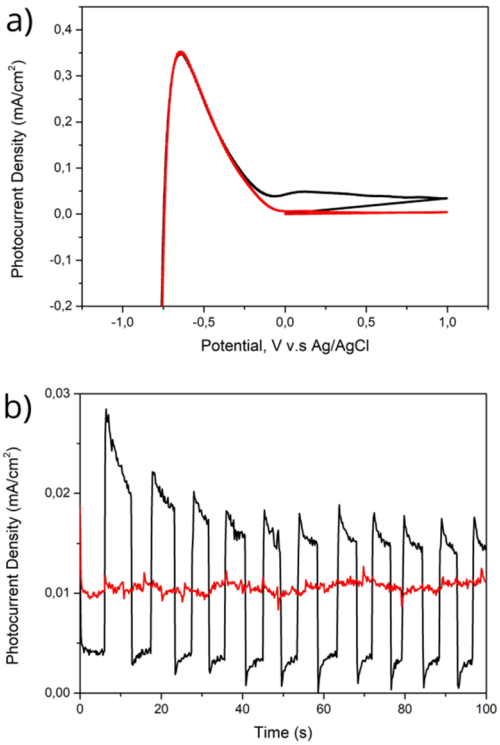

Fig. 8 (a) *I*–*V* graph (b) *I*–*t* curve under illumination conditions of ▬ UV light and ▬ visible light from TNAs prepared at 40 V for 60 minutes and 40 V for 30 minutes, using a Na_2SO_4 electrolyte solution.

The photoelectrochemical performance of MoO_2/TNAs with various variations was tested using irradiation in the visible light region. The photoelectrochemical method applied in this study was the measurement of photocurrent *versus* potential (LSV). Photocurrent was generated through the application of a potential sweep. Meanwhile, transient photocurrent was obtained from irradiation at a constant potential and specific wavelength in the form of a short light pulse (MPA), which aimed to determine charge kinetics, such as the electron diffusion coefficient and the electron transport time from the photocatalyst to the substrate.

Based on the results of linear sweep voltammetry (LSV) measurements in Fig. 9, the photoelectrochemical performance of pure TNAs and MoO_2/TNAs composite materials with 7 SILAR cycles was observed under various precursor concentrations and thermal conditions (argon *vs.* non-argon) under visible light irradiation.

From the curve, the pure TNAs sample (black line) shows the lowest photocurrent density with illumination of visible light. However, when TNAs are modified with MoO_2, it can be seen that there is a change in photocurrent characteristics depending on the concentration of the Mo precursor solution and thermal conditions. The MoO_2/TNAs sample with a precursor concentration of 50 mM under non-argon conditions showed a relatively higher positive photocurrent compared to other variations, especially in the positive potential range up to approximately +0.13 V. Although it did not exceed the peak photocurrent of pure TNAs at negative potentials, the trend of

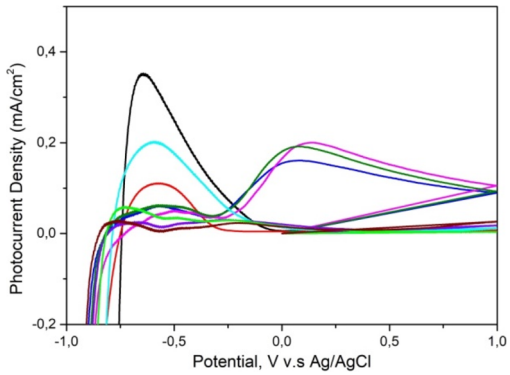

Fig. 9 Graph *I*–*V* under visible light illumination conditions from TNAs 40 V 60 minutes 40 V 30 minutes, MoO_2/TNAs 10 mM, MoO_2/TNAs 30 mM, MoO_2/TNAs 50 mM, MoO_2/TNAs 70 mM, MoO_2/TNAs 10 mM (argon), MoO_2/TNAs 30 mM (argon), MoO_2/TNAs 50 mM (argon), MoO_2/TNAs 70 mM (argon) in Na_2SO_4 electrolyte solution.

photocurrent stability in the positive potential region of 50 mM non-argon MoO_2 showed an increase in charge transfer efficiency and better electron–hole pair separation compared to other variations.

Based on the results of previous UV-Vis DRS characterization, it is known that materials with a concentration of 50 mM non-argon also show the highest absorbance and a shift in light absorption to the visible region (redshift), indicating greater light absorption efficiency and the contribution of electronic transitions from MoO_2 to the TiO_2 structure. The addition of MoO_2 to TNAs can improve photoelectrochemical performance through two main mechanisms, namely the formation of a type II heterojunction between MoO_2 and TiO_2 that facilitates charge separation and increased absorbance in the visible region due to the contribution of Mo^{4+}, which is capable of broadening the light absorption spectrum.

Based on Fig. 10 of the MPA measurement results, pure TNAs electrodes showed a low photocurrent response with

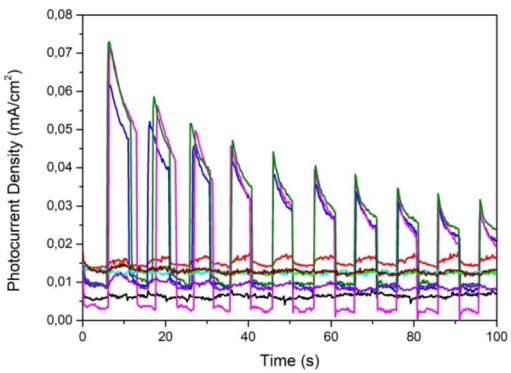

Fig. 10 Graph *I*–*t* under visible light illumination conditions from TNAs 40 V 60 minutes 40 V 30 minutes, MoO_2/TNAs 10 mM, MoO_2/TNAs 30 mM, MoO_2/TNAs 50 mM, MoO_2/TNAs 70 mM, MoO_2/TNAs 10 mM (argon), MoO_2/TNAs 30 mM (argon), MoO_2/TNAs 50 mM (argon), MoO_2/TNAs 70 mM (argon) in Na_2SO_4 electrolyte solution.

a photocurrent density of only about 0.00936 mA cm^{-2}, indicating limited photoelectrochemical activity due to the properties of anatase TiO_2, which has a band gap of about 3.2 eV and is mainly active in the ultraviolet region.[7] Photocurrent density of TNAs pristine higher in UV illumination, but not respond to visible light. The increased current density observed for the MoO_2/TNAs electrode originates from synergistic improvements in charge separation efficiency, electrical conductivity, and optical absorption. The incorporation of conductive MoO_2 enables rapid electron extraction from TNAs, effectively suppressing interfacial recombination. Furthermore, MoO_2 modification narrows the effective band gap and enhances interfacial charge transfer kinetics, thereby significantly improving the photoelectrochemical response.

After modification with MoO_2 using the 7-cycle SILAR method, there was a significant increase in photocurrent density across all concentration variations. Variations in MoO_2 concentration affect charge transfer efficiency. Among all samples tested, MoO_2/TNAs with a concentration of 50 mM in non-argon conditions produced the highest photocurrent density of 0.055 mA cm^{-2}, indicating a substantial increase in efficiency. This indicates that a concentration of 50 mM is capable of producing an ideal structure to support the formation of a semiconductor junction (heterojunction) between MoO_2 and TiO_2, which plays a role in improving electron–hole pair separation and accelerating charge transfer to the substrate.

The lower photocurrent value at a concentration of 70 mM indicates that excess deposition can inhibit charge transfer due to partial closure of the active surface of TiO_2 or the formation of MoO_2 particle agglomerates. This can increase the electron–hole recombination rate, thereby reducing photocurrent efficiency even though light absorption increases.[25]

These MPA results are consistent with the UV-Vis DRS characterization data, where the 50 mM non-argon sample exhibits high visible light absorption and a shift in the absorption band toward longer wavelengths (redshift). This change indicates a narrowing of the band gap, which increases the material's ability to absorb photons from the visible light spectrum and generate more electron–hole pairs.

4 Conclusions

Modification of TNAs with MoO_2 using the SILAR method successfully reduced the band gap from 3.21 eV to 1.56 eV, which expanded light absorption to the visible region. Photoelectrochemical testing using a potentiostat with the LSV and MPA methods showed that the MoO_2/TNAs electrode had a higher current density than pure TNAs, indicating an increase in charge separation efficiency and photoelectrocatalytic activity.

Author contributions

D. N. M.: writing – original draft, data curation, formal analysis, investigation, and S. K. W. N.: conceptualization, data curation,

funding acquisition, project administration, supervision, validation, writing review and editing.

Conflicts of interest

There are no conflicts to declare.

Data availability

Data will be made available on request.

Acknowledgements

The authors would like thank Universitas Negeri Padang for financial support toward the APC of this article, funded by the EQUITY Kemdiktisaintek Program supported by LPDP, under contract number 4310/B3/DT.03.08/2025 and 2692/UN35/KS/2025.

References

1 A. Pratap and R. Shrivastava, Role of graphene and its oxide in heterogeneous photocatalysts for degradation of organic dyes pollutants : Recent advancements and key challenges, *Microchem. J.*, 2025, **219**, 116149, DOI: 10.1016/j.microc.2025.116149.

2 M. A. Al-Nuaim, A. A. Alwasiti and Z. Y. Shnain, The photocatalytic process in the treatment of polluted water, *Chem. Pap.*, 2023, **77**, 677–701, DOI: 10.1007/s11696-022-02468-7.

3 Q. Cheng, Y.-J. Yuan, R. Tang, Q.-Y. Liu, L. Bao, P. Wang, *et al.*, Rapid Hydroxyl Radical Generation on (001)-Facet-Exposed Ultrathin Anatase TiO2 Nanosheets for Enhanced Photocatalytic Lignocellulose-to-H2 Conversion, *ACS Catal.*, 2022, **12**, 2118–2125, DOI: 10.1021/acscatal.1c05713.

4 E. Isik, L. B. Tasyurek, I. Isik and N. Kilinc, Synthesis and analysis of TiO2 nanotubes by electrochemical anodization and machine learning method for hydrogen sensors, *Microelectron. Eng.*, 2022, **262**, 111834, DOI: 10.1016/j.mee.2022.111834.

5 R. Guo, Y. Bao, Q. Kang, C. Liu, W. Zhang and Q. Zhu, Solvent-controlled synthesis and photocatalytic activity of hollow TiO2 microspheres prepared by the solvothermal method, *Colloids Surf., A*, 2022, **633**, 127931, DOI: 10.1016/j.colsurfa.2021.127931.

6 P. Roy, S. Berger and P. Schmuki, TiO2 Nanotubes: Synthesis and Applications, *Angew. Chem., Int. Ed.*, 2011, **50**, 2904–2939, DOI: 10.1002/anie.201001374.

7 S. K. W. Ningsih, M. I. Syauqi, R. Wibowo and J. Gunlazuardi, Effect of potential variation on morphology and photoelectrochemical properties of TiO2 nanotube arrays (TNAs) by two-step anodization method, *J. Appl. Electrochem.*, 2024, **54**, 739–756, DOI: 10.1007/s10800-023-01999-5.

8 Q. Wang, H. Li, X. Yu, Y. Jia, Y. Chang and S. Gao, Morphology regulated Bi_2WO_6 nanoparticles on TiO_2 nanotubes by solvothermal Sb 3p doping as effective photocatalysts for wastewater treatment, *Electrochim. Acta*, 2020, **330**, 135167, DOI: 10.1016/j.electacta.2019.135167.

9 Q. Wang, S. Zhao, Y. Zhao, Y. Deng, W. Yang, Y. Ye, *et al.*, Construction of Z-scheme Bi_2O_3/CeO_2 heterojunction for enhanced photocatalytic capacity of TiO_2 NTs, *Spectrochim. Acta, Part A*, 2024, **304**, DOI: 10.1016/j.saa.2023.123405.

10 Q. Wang, S. Zhu, S. Zhao, C. Li, R. Wang and D. Cao, Construction of Bi-assisted modified CdS/TiO_2 nanotube arrays with ternary S-scheme heterojunction for photocatalytic wastewater treatment and hydrogen production, *Fuel*, 2022, **322**, 124163, DOI: 10.1016/j.fuel.2022.124163.

11 S. Jemai, K. Choubani, A. Hajjaji, S. Sassi, M. B. Rabha, M. A. Almeshaal, *et al.*, Photoactive TiO2 Nanotubes and SILAR-Synthesized PbS/TiO_2 Heterojunctions for Tetracycline Antibiotic Photodegradation, *Inorganics*, 2025, **13**, 1–21.

12 B. Bouktif, M. Rashid, A. Hajjaji, K. Choubani, N. H. Alrasheedi, B. Louhichi, *et al.*, High-Performance Gas Sensor Applications, *Crystals*, 2024, **14**, 1–12.

13 D. Mouloua, N. S. Rajput, J.-F. Blach, M. Lejeune, M. El Marssi, M. A. El Khakani, *et al.*, Fabrication control of MoS_2/MoO_2 nanocomposite *via* chemical vapor deposition for optoelectronic applications, *Mater. Sci. Eng., B*, 2022, **286**, 116035, DOI: 10.1016/j.mseb.2022.116035.

14 J. Hou, L. Gan, N. Bao, C. Zhang, K. Liu and Q. Wang, SILAR-assisted synthesis of Cu_2O modified TiO_2 nanotube arrays: Study on efficient photocatalytic dye degradation and hydrogen evolution, *J. Water Process Eng.*, 2024, **68**, 106364, DOI: 10.1016/j.jwpe.2024.106364.

15 S. K. W. Ningsih, R. Wibowo and J. Gunlazuardi, Photoelectrochemical performance of $BiOI/TiO_2$ nanotube arrays (TNAs) p–n heterojunction synthesized by SILAR-ultrasonication-assisted methods, *R. Soc. Open Sci.*, 2023, **10**(6), 221563, DOI: 10.1098/rsos.221563.

16 H. Budiman, R. Wibowo, O. Zuas and J. Gunlazuardi, Photoelectrochemical properties of TiO_2 nanotube arrays: Effect of different polishing method of Ti substrate prior to anodization in fluoride-H_2O_2-containing electrolyte, *J. Phys.:Conf. Ser.*, 2019, **1153**(1), 012073, DOI: 10.1088/1742-6596/1153/1/012073.

17 N. Pishkar, M. Ghoranneviss, Z. Ghorannevis and H. Akbari, Study of the highly ordered TiO_2 nanotubes physical properties prepared with two-step anodization, *Results Phys.*, 2018, **9**, 1246–1249, DOI: 10.1016/j.rinp.2018.02.009.

18 X. Jing, H. Bai, Y. Zhao, D. Luo and X. Zhang, Schottky-junction MoO2@MoO_3 nanotube arrays: in-situ preparation and photocatalytic activity, *Mater. Chem. Phys.*, 2026, 132110, DOI: 10.1016/j.matchemphys.2026.132110.

19 Y. Etafa Tasisa, T. Kumar Sarma, R. Krishnaraj and S. Sarma, Band gap engineering of titanium dioxide (TiO2) nanoparticles prepared *via* green route and its visible light driven for environmental remediation, *Results Chem.*, 2024, **11**, 101850, DOI: 10.1016/j.rechem.2024.101850.

20 H. Budiman, R. Wibowo, O. Zuas and J. Gunlazuardi, Preparation of TiO_2 Nanotube using Anodization Method: Characterization and Its a Application for Co Sensor,

EduChemia, 2021, **6**, 159–171, DOI: 10.30870/educhemia.v6i1.10793.

21 X. Wang, Y. Liu, J. Zeng, C. Peng and R. Wang, MoO_2/C hollow nanospheres synthesized by solvothermal method as anode material for lithium-ion batteries, *Ionics*, 2019, **25**, 437–445, DOI: 10.1007/s11581-018-2765-2.

22 D. Mouloua, N. S. Rajput, J. Blach, M. Lejeune, M. E. Marssi, M. A. E. Khakani, *et al.*, Materials Science & Engineering B Fabrication control of MoS_2/MoO_2 nanocomposite *via* chemical vapor deposition for optoelectronic applications, *Mater. Sci. Eng., B*, 2022, **286**, 116035, DOI: 10.1016/j.mseb.2022.116035.

23 M. Šćepanović, S. Aškrabić, V. Berec, A. Golubović, Z. Dohčević-Mitrović, A. Kremenović, *et al.*, Characterization of La-Doped TiO_2 nanopowders by Raman spectroscopy, *Acta Phys. Pol. A*, 2009, **115**, 771–774, DOI: 10.12693/APhysPolA.115.771.

24 Y. Xiong, S. Ma, X. Hong, J. Long and G. Wang, Photoelectrocatalytic Processes of TiO2 Film: The Dominating Factors for the Degradation of Methyl Orange and the Understanding of Mechanism, *Molecules*, 2023, **28**, 7967, DOI: 10.3390/molecules28247967.

25 B. Bozkurt Çirak and Ç. Eden, Synthesis, Characterization and Photoelectrochemical Properties of MoS2 decorated TiO2 Nanotubes Electrodes, *Suleyman Demirel Univ. Fen Edebiyat Fak. Fen Derg.*, 2021, **16**, 279–286, DOI: 10.29233/sdufeffd.926533.